Crothers, D. M., Cole, P. E., Hilbers, C. W., & Shulman, R. G. (1974) *J. Mol. Biol. 87*, 63–88.
Davanloo, P., Sprinzl, M., & Cramer, F. (1979) *Biochemistry 18*, 3189–3199.
Davis, G. E., Gehrke, C. W., Kuo, K. C., & Agris, P. F. (1979) *J. Chromatogr. 173*, 281–298.
Freeman, R., & Hill, H. D. W. (1971) *J. Chem. Phys. 54*, 3367–3377.
Gehrke, C. W., Kuo, K. C., McCune, R. A., Gerhardt, K. O., & Agris, P. F. (1982) *J. Chromatogr. 230*, 297–308.
Hall, R. (1971) *The Modified Nucleosides in Nucleic Acids*, Columbia University Press, New York.
Hamill, W. D., Jr., Horton, W. J., & Grant, D. M. (1980) *J. Am. Chem. Soc. 102*, 5454–5458.
Holbrook, S. R., Sussman, J. L., Warrant, R. W., & Kim, S.-H. (1978) *J. Mol. Biol. 123*, 631–660.
Kan, L. S., Ts'o, P. O. P., Sprinzl, M., Von der Haar, F., & Cramer, F. (1977) *Biochemistry 16*, 3143–3153.
Komoroski, R. A., & Allerhand, A. (1972) *Proc. Natl. Acad. Sci. U.S.A. 69*, 1804–1808.
Komoroski, R. A., & Allerhand, A. (1974) *Biochemistry 13*, 369–372.
Kopper, R. A., Schmidt, P. G., & Agris, P. F. (1983) *Biochemistry* (first paper of three in this issue).
London, R. E. (1980) in *Magnetic Resonance in Biology* (Cohen, J. S., Ed.) pp 1–69, Wiley, New York.
Patkowski, A., & Chu, B. (1979) *Biopolymers 18*, 2051–2072.
Pitner, T. P., & Glickson, J. D. (1975) *Biochemistry 14*, 3083–3087.
Schmidt, P. G., & Edelheit, E. B. (1981) *Biochemistry 20*, 79–86.
Schmidt, P. G., Tompson, J. G., & Agris, P. F. (1980) *Nucleic Acids Res. 8*, 643–656.
Schmidt, P. G., Playl, T., & Agris, P. F. (1983) *Biochemistry* (third paper of three in this issue).
Schweizer, M. P., Hamill, W. D., Jr., Walkiw, I. J., Horton, W. J., & Grant, D. M. (1980) *Nucleic Acids Res. 8*, 2075–2083.
Sprinzl, M., & Gauss, D. (1982) *Nucleic Acids Res. 10*, r1–r55.
Sussman, J. L., Holbrook, S. R., Warrant, R. W., Church, G. M., & Kim, S.-H. (1978) *J. Mol. Biol. 123*, 607–630.
Tompson, J. G., & Agris, P. F. (1979) *Nucleic Acids Res. 7*, 765–779.
Tompson, J. G., Hayashi, F., Paukstelis, J. V., Loeppky, R. N., & Agris, P. F. (1979) *Biochemistry 18*, 2079–2085.
Woessner, D. E. (1962) *J. Chem. Phys. 36*, 1–4.
Yokoyama, S., Usuki, K. M. J., Yamaizumi, Z., Nishimura, S., & Miyazawa, T. (1980) *FEBS Lett. 119*, 77–80.

Internal Dynamics of Transfer Ribonucleic Acid Determined by Nuclear Magnetic Resonance of Carbon-13-Enriched Ribose Carbon 1†

Paul G. Schmidt, Timothy Playl, and Paul F. Agris*

ABSTRACT: Carbon-13 enrichment of the C1′ position of the ribose moiety in *Escherichia coli* tRNA has made possible the detailed study of motion in this molecule. Enrichment was accomplished in vivo with a strain, M1R, selected for growth and degree of incorporation of ribose in a stringently defined minimal medium. Purine biosynthesis de novo was blocked with 6-mercaptopurine. Exogenously provided [1-^{13}C]ribose and nucleobases were utilized via the salvage pathway and were required for growth of culture. Carbon-13-enriched transfer RNA in solution at 30 °C exhibited a prominent, broad, asymmetric NMR signal at 91.5 ppm for the C1′ carbon. Upon heat denaturation of the tRNA, three C1′ signals were resolved and could be attributed to the base-specific nucleotides in tRNA: uridine and guanosine at 88.7 ppm; adenosine at 89.5 ppm; and cytidine at 90.6 ppm. Ribose C3′ and C5′ were partially enriched due to scrambling of ribose carbons in vivo. The minimum net isotopic enrichment of C1′ was 33%. Values for the relaxation time T_1 and the nuclear Overhauser enhancement (NOE) at 75.5, 67.8, and 25.2 MHz (^{13}C), the NOE at 50.3 MHz, T_2 at 75.5 MHz, and line widths over the range of 20–75.5 MHz were analyzed in light of several models for internal motion in macromolecules. The data were inconsistent with physically unreasonable constructs involving free internal diffusion of the C1′–H vector about the glycosidic bond. Internal diffusion (wobble) within a cone or jumps between states were models that did fit the data. For diffusion within a cone, the cone half-angle was 15–20°, with a correlation time of about 2×10^{-9} s for internal reorientation. With the two-state jump model, the half-angle for jumps about the glycosidic bond was $14 \pm 2°$ with a lifetime of 2×10^{-9} s.

The ability of macromolecules to interact specifically and successfully in enzymatic reactions is dependent on pliant conformational recognition in three dimensions. Thus, we need to understand not only structure but also structural flexibility and motional capability, particularly internal motion (London, 1980), which is important for mechanisms of catalysis or receptor activation. Nuclear magnetic resonance (NMR) and fluorescence are the techniques most suited for measuring internal motions in macromolecules. Fluorescence is superior from the standpoint of signal sensitivity, but NMR has the advantage of generally offering a nonperturbing probe. Sensitivity limitations are particularly acute in NMR of ^{13}C (1.1% natural abundance), yet it is the nucleus of choice in most dynamic NMR studies of biological molecules, since its re-

† From the Division of Biological Sciences, University of Missouri, Columbia, Missouri 65211 (T.P. and P.F.A.), and the Oklahoma Medical Research Foundation and the Department of Biochemistry and Molecular Biology, University of Oklahoma Health Sciences Center, Oklahoma City, Oklahoma 73104 (P.G.S.). *Received August 2, 1982.* This research was financially supported by Research Grants GM23037 from the National Institutes of Health to P.F.A. and GM25261 to P.G.S. P.G.S. acknowledges receipt of a Research Career Development Award (AM00525), and P.F.A. acknowledges receipt of a National Research Service Award Senior Fellowship (F33-GM07826), both from the National Institutes of Health.

0006-2960/83/0422-1408$01.50/0

laxation times are more easily interpreted than those of ^{1}H and ^{31}P, the other most observed nuclei. It has proved quite advantageous to enrich site-specific locations within biological macromolecules with ^{13}C-labeled residues, and numerous studies of labeled proteins have been published (Blakley et al., 1978; Otvos & Browne, 1980; Jelinski & Torchia, 1980; Moore & Browne, 1980). Labeling a molecule by enrichment of the native structure with ^{13}C does not disrupt conformation nor hinder biological activity in any way, whereas labeling with other probes can create structural artifacts.

The first ^{13}C enrichment of a nucleic acid with the retention of native structure was accomplished through the in vivo methylation of *Escherichia coli* tRNA from exogenously provided [^{13}C]methylmethionine (Agris et al., 1975). Purified species of tRNA yielded single-carbon resonance resolution of methyl signals (Agris & Schmidt, 1980). Nishimura and co-workers have also reported spectra of [^{13}C]methyl-enriched *E. coli* tRNAs (Yokoyama et al., 1980). Carbon-13-labeled metabolites have been used to enrich the C2 positions of adenosine, cytidine, and uridine in tRNA (Tompson & Agris, 1979). Spectra produced by the in vivo enrichment technique showed prominent signals, allowing analysis of longitudinal and transverse relaxation times, T_1 and T_2, and the nuclear Overhauser effect, NOE (Schmidt et al., 1980). Enrichment techniques have been used to label the C4 position of uridine in tRNA. Single-carbon resonance resolution has been obtained in spectra of *E. coli* $tRNA_1^{Val}$ (Schweizer et al., 1980). Thus, previous research utilizing enrichment techniques has concentrated on producing spectra from various ^{13}C-labeled positions on the nucleobases.

In this paper, we present, for the first time, techniques for ^{13}C enrichment of the ribose moiety of tRNA. Study of ^{13}C NMR relaxation parameters of tRNA sugar residues at four different Larmor frequencies enabled analysis of internal motion based, in part, on recent treatments of deoxyribose in DNA (Lipari & Szabo, 1981; Keepers & James, 1982). Key advantages of isotopic enrichment are seen in the increased accuracy of relaxation times and NOE values because of greater signal-to-noise levels and in the ability to obtain relaxation data at lower magnetic fields (2.35 T) where previous natural abundance tRNA spectra showed marginal signal levels. The present work deals with enrichment of C1′ of ribose; these and future data on ^{13}C at other sugar positions promise to help bring into balance the present situation where an abundance of high-powered theoretical treatments are trained on precious little data.

Materials and Methods

Escherichia coli C6 rel$^-$met$^-$cys$^-$ strain M1R was grown in a stringently defined minimal medium at 37 °C in an Orbit Environ-Shaker. The culture medium consisted of 22.2 mM KH_2PO_4 and 42.4 mM Na_2HPO_4 (pH 7.0), 18.7 mM NH_4Cl, 1.91 mM $MgSO_4$, 2.2 μM $FeSO_4$, 0.496 mM $CaCl_2$, 27.7 mM ribose (or [1-^{13}C]ribose), 0.01 mM 6-mercaptopurine, 0.10 mM methionine, 0.178 mM uracil, 0.18 mM cytosine, 0.11 mM guanine, and 0.054 mM adenine. [1-^{13}C]Ribose was obtained from the Stable Isotope Resource, Los Alamos Scientific Laboratory, Los Alamos, NM. The degree of ^{13}C enrichment (86 atom %) was confirmed by high-resolution single-ion-monitoring mass spectrometry and ^{13}C NMR spectroscopy. The cells were tested for ribose dependency prior to inoculation of the medium. Culture growth was followed spectrophotometrically by measuring transmission at 550 nm.

Cultures of 150 and 800 mL containing the ^{13}C-labeled ribose were harvested by centrifugation when the cells were in late log phase of growth, approximately 9 h after inoculation. Nucleic acids were extracted by standard methods. The bulk tRNA enriched with [^{13}C]ribose was then isolated by DEAE-cellulose[1] chromatography (Tompson et al., 1979), precipitated with ethanol, dissolved in glass-distilled water, and dialyzed extensively against glass-distilled water for 4 h with the water changed every 30 min to facilitate removal of all the ethanol. The tRNA solutions were concentrated by evaporation under vacuum to near dryness. Then, they were redissolved in H_2O/D_2O (1:1) to final volumes of either 2.0 or 0.5 mL to give tRNA concentrations of approximately 0.52 or 2.1 mM, respectively, in preparation for NMR spectroscopy.

NMR spectra at 75.5 MHz (^{13}C) were collected in a quadrature-detection Fourier-transform spectrometer of hybrid construction composed of a CMS 70/50 magnet and 10-mm probe (Cyromagnet Systems, Indianapolis, IN), a Nicolet 1180 computer, a Bruker temperature control unit, and in-house radio-frequency gear. Spectroscopy at 67.9 MHz was done with the same console and computer equipped with a Bruker 63.4-kG magnet; experiments at 25.16 MHz employed a Varian XL-100 spectrometer, modified for the Fourier-transform mode by Nicolet. Spectra at 50.3 MHz were obtained on a JEOL FX-200 instrument.

Longitudinal relaxation times were measured by the inversion–recovery method with 7–8 delay periods. The data were fit to exponential decays with a three-parameter analysis routine (Kowalewski & Levy, 1977) on the Nicolet 1180 computer. NOE measurements were done by the gated decoupling method with wait times between pulses of at least $5T_1$ (of ^{13}C). Longer delay times were checked (at 75.5 MHz) and found not to change the NOE value. Transverse relaxation times (T_2) were measured by the Carr–Purcell method with variable pulse delay to monitor the decay of magnetization. Experiments with and without proton noise decoupling gave similar results (Freeman & Hill, 1975).

Results

Cell Cultures. E. coli strain M1R, derived from strain M1 used in previous enrichment studies (Tompson & Agris, 1979), was selected for growth and ribose incorporation in the minimal medium described under Materials and Methods. Purine biosynthesis de novo and adenosine–guanosine interconversion were blocked with the drug 6-mercaptopurine at a concentration of 0.01 mM. Cell growth was dependent upon ribose concentration with the optimum conditions being 27.7 mM ribose. Figure 1 demonstrates the effects of increasing ribose concentration on growth of cultures in the presence of 6-mercaptopurine and nucleobases. Addition of increasing amounts of ribose continually improved growth of cultures. At concentrations of 27.7 mM ribose, the rate and extent of growth approximated that of a culture grown in excess ribose. Ribose incorporation into acid-precipitable material was determined with [1-^{14}C]ribose (sp act. 0.6 μCi/μmol). This incorporation paralleled the growth of cultures (Figure 2).

A 950-mL culture of *E. coli* strain M1R was grown in medium containing [1-^{13}C]ribose. The cells were collected after 9 h, and the bulk tRNA was extracted from the cells. The packed cells (4.56 g wet wt) yielded approximately 32.5 mg of bulk tRNA.

^{13}C NMR Spectra. [1-^{13}C]Ribose was synthesized (Serianni et al., 1980) and provided by Los Alamos Scientific Laboratory Stable Isotope Resource. Complete limitation of enriched carbon to the C1 position and extent of enrichment (86 atom %) were confirmed by NMR and mass spectrometry (Figure

[1] Abbreviations: DEAE, diethylaminoethyl; HPLC, high-performance liquid chromatography; FID, free-induction decay.

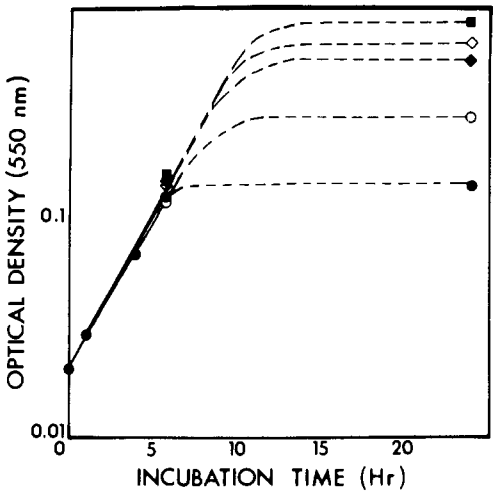

FIGURE 1: Growth dependence of *E. coli* M1R on ribose. Ribose concentrations were varied from 1.4 (●) to 4.2 (○), to 8.4 (♦), to 14 (◇), and to 28 (■) mM.

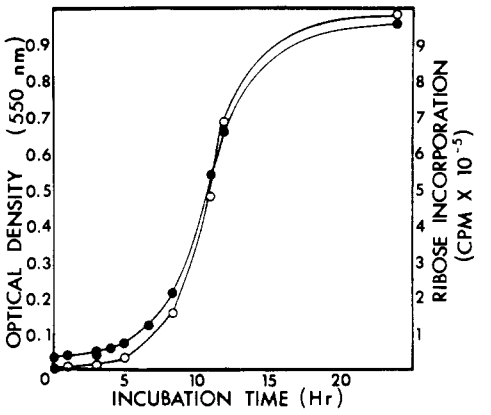

FIGURE 2: Incorporation of [1-^{14}C]ribose into acid-precipitable material of *E. coli* M1R. The closed circles (●) represent culture growth of *E. coli* in 8.4 mM ribose (0.6 μCi/μmol). Incorporation of the radioactive label into macromolecules follows the culture growth and is represented by open circles (○).

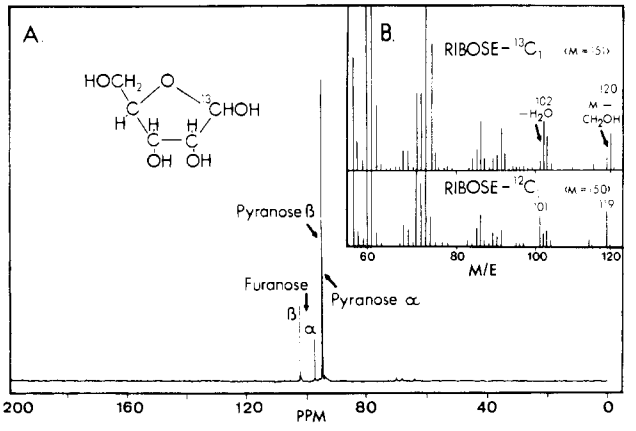

FIGURE 3: Mass spectra and NMR of synthetic ^{13}C1-labeled ribose precursor: (A) ^{13}C NMR spectrum of labeled ribose in D_2O; 15 MHz, ambient temperature, tetramethylsilane = 0 ppm. (B) Mass spectrum. Lower panel is for unenriched compound, upper panel is for synthetic [1-^{13}C]ribose. Two major fragments and their mass numbers are indicated.

3). For the furanose form, β and α isomers are at 102.6 and 97.9 ppm; in the pyranose structure the corresponding isomers are at 95.4 and 95.1 ppm. The four peak heights were found to be characteristics of an equilibrium mixture of mutarotated D-ribose (Breitmaier & Hollstein, 1976).

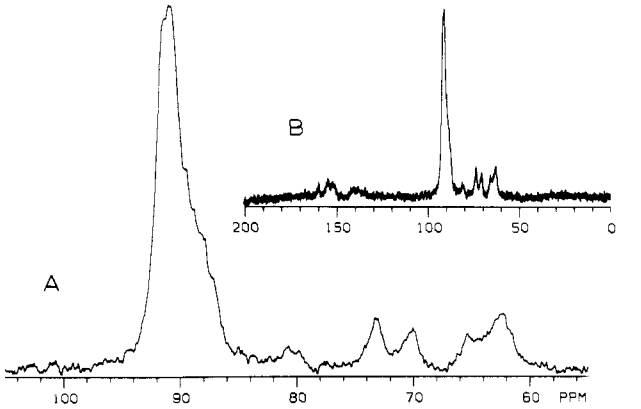

FIGURE 4: 75.5-MHz ^{13}C NMR spectrum of [1-^{13}C]ribose-labeled *E. coli* tRNA: (A) ribose carbon region; (B) full spectrum. Sample was 2.1 mM in 0.5 mL of D_2O/H_2O; 10 mM $MgCl_2$, 30 °C. A microcell was used, held in a 10-mm tube. 4200 scans; 1.45-s delay between pulses; 90° pulse. Digital filtering of 5 Hz on the free induction decay. 8K points, zero-filled to 16K.

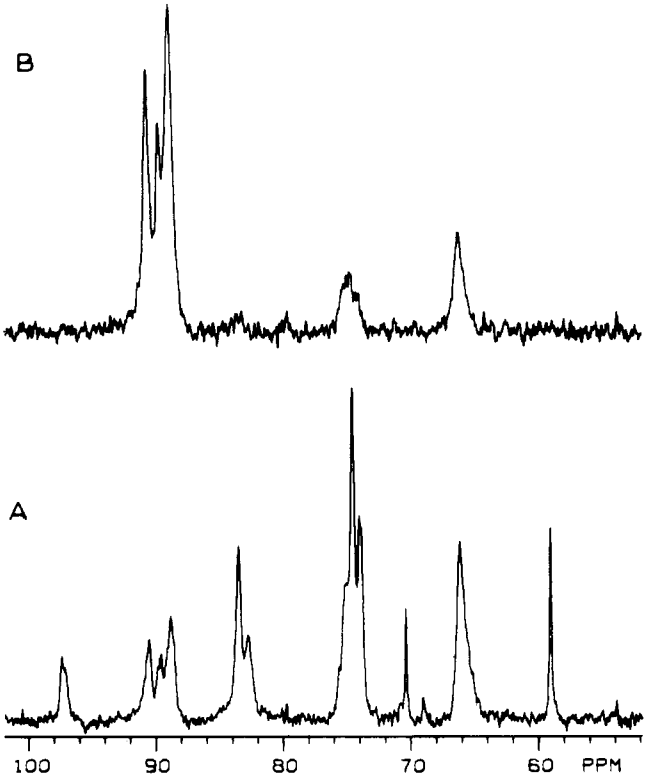

FIGURE 5: NMR spectra of tRNA at 80 °C. (A) Sample of tRNA enriched in ^{13}C in methyl groups (*not* in ribose). Approximately 1 mM in D_2O/H_2O, no added $MgCl_2$ or salt. 75.5 MHz; 46 080 scans; 1-s pulse time; 55° pulses; 16K points in time domain; 5-Hz line broadening. (B) [1-^{13}C]Ribose-enriched tRNA. 0.5 mM in D_2O/H_2O, no added $MgCl_2$ or salt. 67.9 MHz; 1000 scans; 0.28-s pulse delay time; 55° pulses; 16K points; 5-Hz broadening.

Figure 4 is a 75.5-MHz spectrum of the ^{13}C-enriched tRNA sample in D_2O/H_2O with 10 mM $MgCl_2$ added. The signal-to-noise advantage of specific enrichment is obvious for the C1′-ribose peak near 90 ppm. Signals from the other ribose carbons appear upfield of C1′ with nucleobase carbons downfield, most between 130 and 160 ppm (Tompson et al., 1979).

A spectrum of the ^{13}C1′-enriched tRNA sample without added Mg^{2+} was taken at 80 °C where the polynucleotide chains are mostly unfolded (Figure 5B). In this 67.9-MHz spectrum, three peaks are resolved in the C1′ band and, by comparison with dinucleotide chemical shifts (J. L. Alderfer,

Table I: Relaxation Parameters for C1′ of *E. coli* tRNA[a]

f_0 (MHz)	T_1[b] (s)	T_2[c] (s)	NOE[d] $(1+\eta)$	$W_{1/2}$[e] (Hz)
25.16	0.12		1.37	88 (118)[f]
50.3[g]			1.20	147
67.9	0.41	0.14	1.29	177
75.5	0.48	0.10	1.26	204 (193)[f]
20.1				80

[a] Sample 2.1 mM in D_2O/H_2O, 10 mM $MgCl_2$, 30 ± 2 °C. [b] Estimated experimental uncertainty ±10%. [c] Estimated experimental uncertainty ±25%. [d] Estimated experimental uncertainty ±0.05. [e] Estimated experimental uncertainty ±20%. [f] Values in parentheses are for measurements on separate spectra. [g] Temperature ca. 22 °C.

private communication), are assigned to uridine and guanosine (88.7 ppm), adenosine (89.5), and cytidine (90.6).

Degree of Isotopic Enrichment. The relative areas of ribose carbons offer a clue to the final extent of ^{13}C enrichment at C1′ and to the metabolic fate of ribose when used as the sole carbon source in our cell cultures. In a comparison of spectra from heat-denatured natural abundance ^{13}C tRNA (Figure 5A) to that of $^{13}C1'$-enriched tRNA (Figure 5B), the 5′ (at 66 ppm) and 3′ (and/or 2′) positions (at 74–75 ppm) were found to be substantially enriched compared to the 4′ peak at 83 ppm. The same trend is seen in the native structure spectrum of enriched tRNA (Figure 4). Area ratios for 1′:4′:2′,3′:5′ are 100:3.4:13.7:15.5 for tRNA at 30 °C (Figure 4) and 100:3.3:14.0:18.4 at 80 °C (Figure 5B). If one considers a lower limit in which the 4′ position has not been enriched at all, the percentage isotopic incorporations (Figure 4) are 33:1.1:4.5:5.0 where the 2′,3′ peak is treated as one locus for the moment.

Limited mass spectral data indicating the amount and distribution of ^{13}C incorporation into these samples was obtained by analysis of nucleosides purified by HPLC of enzymatically hydrolyzed tRNA (Davis et al., 1979). From fragments containing base plus C1′ carbon, $^{13}C/^{12}C$ ratios indicate for Ado 57% enrichment and for Urd 23% enrichment (low levels of these fragments lead to substantial experimental uncertainties). The mass spectra results are approximately consistent with our NMR lower limit, suggesting that indeed 4′ is not enriched. Since ribose is the sole carbon source, conversion to triose and hexose with resynthesis of pentose is quite reasonable. This could lead to scrambling of the enriched carbon, resulting in partial enrichment at 3′ and 5′ but not at 2′ and 4′.

Relaxation Times, NOE Values, and Line Width for C1′. NOE values and line widths at four magnetic field strengths, T_1 at three fields, and T_2 at 7.05 T are listed in Table I. These data are for 2 mM *E. coli* tRNA in the presence of 10 mM $MgCl_2$ at a temperature of 30 ± 2 °C (except the 50.3-MHz NOE where the sample temperature was 22 °C).

Figure 6 displays representative spectra from NOE experiments at 75.5 and 25.2 MHz. T_2 values measured from the decay rate of different parts of the peak at 75.5 MHz are noted on the figure. The major band near 91 ppm relaxes most rapidly (T_2 = 10 ms), and it is this value that was used for data fitting. If one uses the total area of the band, T_2 equals 9.7 ms, well within experimental error of the value based on height at the maximum. Peak shapes with and without NOE are very similar at 75.5 MHz (Figure 6). A slight difference may exist for the peaks in this experiment at 25.5 MHz. In any case, we do not observe any substantial group of peaks whose chemical shift and NOE are simultaneously different from the others.

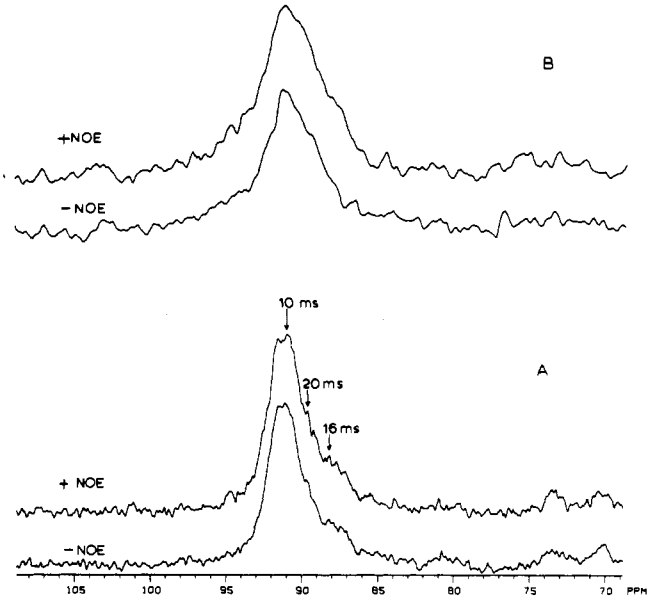

FIGURE 6: NOE experiment. (A) 75.5 MHz: 2.1 mM [1-^{13}C]-ribose-enriched tRNA in a 0.5-mL microcell; 10 mM $MgCl_2$; 26 °C. (Upper trace) Continuous broad-band proton decoupling (100-Hz phase modulation). (Lower trace) Decoupling gated on for FID only. Delay of 2.7 s between pulses. Temperature differences minimized by alternating between series of gated and continuous decoupling modes. (B) 25.16 MHz: Sample as in A; 28 °C. (Upper trace) Continuous noise modulated ^1H decoupling. (Lower trace) Gated decoupling for acquisition only. 2.8-s delay between pulses. Numerical values in (A) are apparent T_2s measured at the positions indicated.

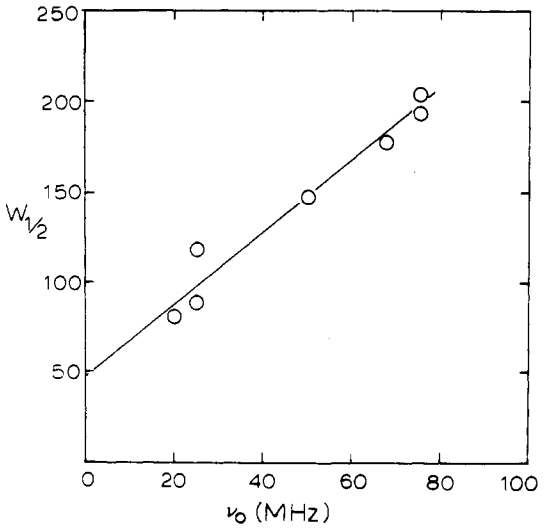

FIGURE 7: Line width vs. Larmor frequency for C1 peak. Full width at half-height is plotted. The line is the least-squares best fit to all the data. Different data points at 25.2 and 75.5 MHz represent line widths measured in separate experiments. Maximum random errors in measurement are estimated at ±10% for the highest frequency and ca. ±20% for the 20.1- and 25.2-MHz data.

At low temperatures where tRNAs are predominantly folded up (25–30 °C), the 75.5-MHz C1′ resonance is broad, asymmetric, and unresolved. Its shape does not reflect the high-temperature peak distribution because of substantial shifts induced in C1′ when tRNAs fold into their native secondary and tertiary structure. The overall width at half-height, $W_{1/2}$ is about 200 Hz at 75.5 MHz after correction for instrumental broadenings. From spectra at 75.5, 67.9, 50.3, 25.2, and 20.1 MHz, $W_{1/2}$ was plotted vs. NMR frequency (Figure 7). Extrapolation to zero frequency yielded an estimate of the true line width without contributions from the spread in chemical shifts. A value of 48 Hz was obtained from the intercept of

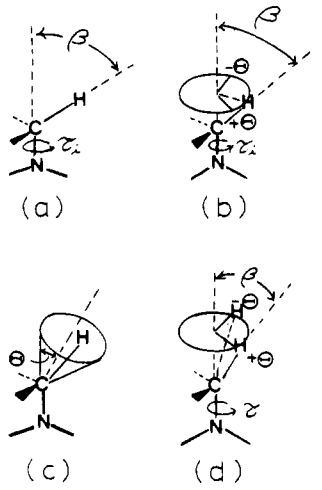

FIGURE 8: Possible modes of internal motion of C1–H internuclear vector. (A) Free internal diffusion through 2π radius around glycosidic bond. (B) Free internal diffusion within a restricted boundary potential well. (C) Diffusion of C–H vector within a cone at half-angle θ. Correlation time used in text for internal motion is ζ_{int}. (D) Two-state jump. ζ is half the lifetime in either state.

this plot (ignoring for the moment possible frequency dependence of intrinsic line widths). With use of only the data above 50 MHz, the intercept is 44 Hz. T_2 values measured by the Carr–Purcell method at 75.5 MHz (see below) are consistent with intrinsic widths of about 32 Hz. If one considers the large errors possible in extrapolating line widths to ν_0 equal to 0, the agreement is reasonable. Transverse relaxation times are frequency dependent, but in the framework of internal motion developed below, the values increase only about 4% from 75.5 to 20 MHz so the frequency dependence of $W_{1/2}$ was ignored in our extrapolation.

Models for Motion. If the C1′–H vectors were rigid with respect to the overall tRNA structure, then the NOE values at each frequency would be 1.15 [given an overall rotational correlation time >15 ns (Schmidt et al., 1980; Patkowski & Chu, 1979)]. The accuracy of our NOE values (e.g., 1.37 ± 0.05 at 25.2 MHz) is sufficient that we can rule out the "rigidly fixed to overall motion" model for C1′ as have previous workers examining yeast tRNA by natural abundance ^{13}C NMR (Bolton & James, 1980a,b).

In recent months, a spate of papers have appeared that deal with models for internal motion in nucleic acids (mostly DNA) designed to rationalize NMR relaxation data (Bolton & James, 1979, 1980a,b; Early & Kearns, 1979; Hogan & Jardetzky, 1979; Lipari & Szabo, 1981; Keepers & James, 1982). As might be expected, these models have progressed in sophistication over time, ranging from free internal diffusion about an axis undergoing isotropic overall reorientation on the basis of the classic paper of Woessner (1962) to multiple internal jumps (Keepers & James, 1982) that may be appropriate for the phosphate and C5′. In considering possibilities for internal motion of the C1′–H bond, we felt that models involving wobbling of the internuclear vector within a cone (Bull et al., 1978; Howarth, 1979; Lipari & Szabo, 1980) or jumps between potential minima (London, 1980; Wittebort & Szabo, 1978) might approximate the actual motion. A model involving free diffusion within restricted boundaries is also plausible (London & Avitable, 1978; Wittebort & Szabo, 1978). Free internal diffusion around the C1′–base nitrogen bond and the almost equivalent jumps with 2π total angular range are physically unreasonable models. But these models have been shown to fit the data in other nucleic acid studies, so we included them for comparison. Overall motion was taken as isotropic although hydrodynamic studies (Patkowski & Chu, 1979) support a nonspherical molecule (vide infra), as does low-angle scattering.

Diagrams of the several models appropriate for the C1′–H internuclear vector of tRNA are shown in Figure 8 where the angular terms and correlation times are illustrated. The base–sugar glycosidic bond is taken as the axis for internal rotations. Origin of motion is not specified, but it could arise from simple rotations of a rigid sugar about the C–N bond or, more likely, from ring pucker or pseudorotation (Levitt & Warshel, 1978). There is evidence to suggest that the base portions of tRNA are fairly rigid relative to the overall tRNA structure (Schmidt et al., 1980; Bolton & James, 1980a,b), but this constraint is not demanded by the "wobble in a cone" model [although, strictly speaking, the C–H axis should coincide with the wobble axis (Lipari & Szabo, 1980)].

Spectral densities for each of these models are as follows:

$$J(\omega)_{cone} = A\frac{\zeta_R}{1 + \omega_0^2\zeta_R^2} + (1 - A)\frac{(1/\zeta_R + 1/\zeta_i)^{-1}}{1 + \omega_0^2(1/\zeta_R + 1/\zeta_i)^{-2}} \quad (1)$$

where

$$A = \frac{\cos^2\theta \sin^4\theta}{4(1 - \cos\theta)^2}$$

$$J(\omega)_{jump} = (1 - C)\frac{\zeta_R}{1 + \omega_0^2\zeta_R^2} + C\frac{(1/\zeta_R + 1/\zeta)^{-1}}{1 + \omega_0^2(1/\zeta_R + 1/\zeta)^{-2}} \quad (2)$$

where

$$C = (3/4)[\sin^2\beta(1 - \cos 2\theta)][2 - \sin^2\beta(1 - \cos 2\theta)]$$

$$J(\omega)_{free} = E\frac{\zeta_R}{1 + \omega_0^2\zeta_R^2} + F\frac{[1/\zeta_R + 1/(6\zeta_i)]^{-1}}{1 + \omega_0^2[1/\zeta_R + 1/(6\zeta_i)]^{-2}} + G\frac{[1/\zeta_R + 2/(3\zeta_i)]^{-1}}{1 + \omega_0^2[1/\zeta_R + 2/(3\zeta_i)]^{-2}} \quad (3)$$

where

$$E = (1/4)[3\cos^2(\beta - 1)]^2 \qquad F = (3/4)(\sin^2 2\beta)$$

$$G = (3/4)(\sin^4\beta)$$

Note that $J(\omega)$ in each of these equations is half the Fourier transform of the rotational autocorrelation function (London, 1980). In all equations, ω_0 is the Larmor frequency, and ζ_R is the overall isotropic rotational correlation time. Other factors are illustrated in Figure 8. In all cases, β was set to 70.5°, the complement of the tetrahedral angle. Note the similarities of spectral-density expressions for wobble in a cone (eq 1) and jumps between angular limits (eq 2). The internal motion correlation times do not have the same meaning, nor do the angular factors. But a best fit of the data to either model provides the solution for the other. At the same time, these models cannot be distinguished from the relaxation data alone. Predicted values for T_1, T_2, and the NOE are calculated by using the spectral densities in the appropriate relaxation equation (London, 1980).

Free Internal Rotation: A Viable Model? In several previous NMR studies of sugar carbons in nucleic acids, an examination was made of a model of free internal diffusion about an axis undergoing overall reorientation. Surprisingly, it was shown to fit the available data for DNA and yeast tRNA (Bolton & James, 1980a,b; Lipari & Szabo, 1981). Of course, the authors pointed out the physical unreasonability of this model for unbroken, stacked polynucleotides, and they have

Table II: Calculated ^{13}C-H Dipolar Relaxation Parameters for Internal Diffusion within a Cone[a]

		25.2 MHz			75.5 MHz		
θ[b]	r_{C-H} (Å)	$1/(NT_1)$[d] (s^{-1})	$1/(NT_2)$ (s^{-1})	NOE $(1+\eta)$	$1/(NT_1)$ (s^{-1})	$1/(NT_2)$ (s^{-1})	NOE $(1+\eta)$
10°	1.09	9.7	128	1.25	1.4	123	1.22
10°	1.11	8.7	114	1.25	1.25	110	1.22
15°	1.09	10.3	121	1.35	1.8	116	1.26
15°	1.11	9.1	109	1.35	1.6	104	1.26
20°	1.09	10.9	113	1.47	2.3	108	1.30
20°	1.11	9.8	102	1.47	2.1	97	1.30
25°	1.09	11.8	105	1.59	2.9	99	1.32
25°	1.11	10.5	94	1.59	2.6	87	1.32
30°	1.09	12.7	94	1.71	3.6	87	1.35
30°	1.11	11.4	84	1.71	3.3	78	1.35
experimental (30 °C, 10 mM Mg^{2+})		8.2		1.37	2.1	100[c]	1.26

[a] Conditions: $\zeta_{int} = 1.6 \times 10^{-9}$ s, $\zeta_R = 30 \times 10^{-9}$ s. [b] Half-angle of cone. [c] Relaxation rate for majority of resonances. [d] N = number of directly bonded protons.

examined other, more likely internal motion possibilities that also work (Lipari & Szabo, 1981; Keepers & James, 1982). We found that the 75.5-MHz relaxation data for C1′ of *E. coli* tRNA did not fit the free internal motion construct. Figure 9 illustrates this with a plot of calculated NOE, $1/(NT_1)$, and $1/(NT_2)$ vs. ζ_{int} for free internal reorientation of a tetrahedral carbon (dashed lines) and wobbling within a cone (solid line). (N equals the number of directly bonded protons.) The half-angle of the cone was set to 18° and ζ_R was set to 30 ns, values that gave the best fit to all the experimental data. The free internal diffusion model does not come close to fitting simultaneously $1/(NT_1)$ and the NOE, nor does it do so for other choices of ζ_R.

Internal Diffusion within a Cone and Two-State Jump Models. Table II lists the best fit parameters for internal and overall motion of C1′ for the wobble in a cone model. Predicted values of $1/T_1$, $1/T_2$, and NOE are given for 25.2 and 75.5 MHz at half-angles of the cone boundary ranging from 10 to 30°. Choice of C–H internuclear distance can be crucial to the solution for a correlation time (Dill & Allerhand, 1979), so two values were tested, 1.09 and 1.11 Å. Use of the larger distance improves the fit of 25.2-MHz T_1 data, but 1.09 Å is a more commonly used value. For overall reorientation, a correlation time of approximately 30 ns gave the best fit; satisfactory fits could be made for values of ζ_R in the range 25–35 ns. T_2 values are most sensitive to the choice of this parameter, and they are the least accurate, so some uncertainty is expected.

NOE values do not depend strongly on ζ_R in the range considered, nor do they depend on choice of bond length. However, the NOE depends strongly on rate and amplitude of internal motion. Given a relatively small experimental uncertainty in the NOE (±0.05), the very close fit of data of 25.2 and 75.5 MHz to predicted enhancements confines internal motion to a fairly narrow range of amplitudes and rates, i.e., between 15 and 20° for the half-angle and 1.6 (±0.5) × 10^{-9} s for the internal reorientation correlation time.

The solution to the wobble in a cone problem also gives the best fit for ζ_R and the internal reorientation time for a two-state jump model because of the similarity in the spectral density expressions (eq 1 and 2). In the jump model, ζ_{int} [1.6 (±0.5) × 10^{-9} s] becomes half the average lifetime in each state, and the best fit of the coefficients in eq 2 yields a half-angle for jumps of $\theta = 14 \pm 2°$.

While the simultaneous fit to all the relaxation data is good, we believe that the discrepancy between predicted and experimental values of T_1 at 25.2 MHz is outside of experimental error. Increasing the value of ζ_R to 35 × 10^{-9} s and using a bond length of 1.11 Å (with $\theta = 18°$ and $\zeta_{int} = 1.6 \times 10^{-9}$ s as before) puts the predicted value of $1/(NT_1) = 8.6$ s^{-1} within experimental error of the observed value, 8.2 s^{-1}. The effect of the above changes on $1/(NT_1)$ at 75.5 MHz is to lower the predicted value to 1.76 s^{-1}, just outside experimental error limits for the observed value of 2.1 s^{-1}. While the wobble in a cone and two-state jump models certainly are not perfect constructs for motion of C1′ in tRNA, they do fit the data quite well.

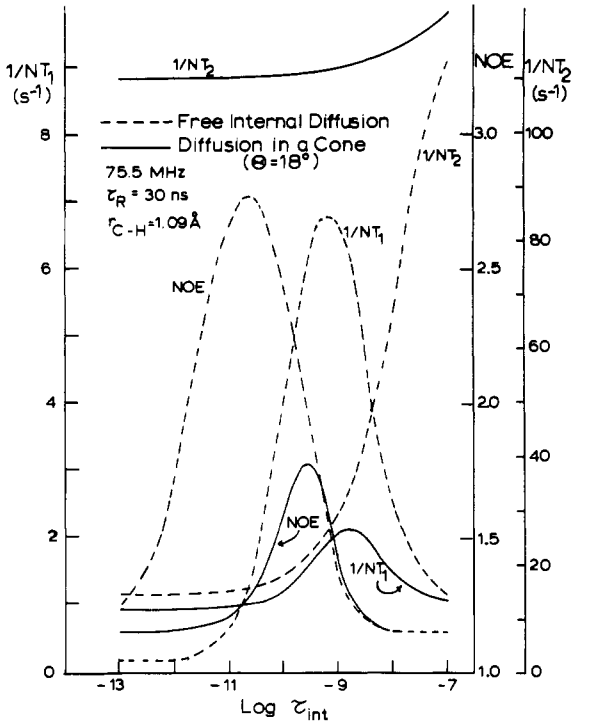

FIGURE 9: Predicted relaxation parameters for diffusion in a cone and free internal diffusion models. Conditions: 75.5 MHz; ζ_R = 30 ns; r_{C-H} = 1.09 Å. (– –) Free internal diffusion for $\beta = 70.5°$ (see Figure 8). (—) Diffusion within a cone of half-angle $\theta = 18°$. N equals the number of directly bonded protons.

The value of $\zeta_R = 30$ ns at 30° compares closely with results of a recent study of yeast tRNA by intensity fluctuation spectroscopy. Patkowski & Chu (1979) found a rotational correlation time ζ_R [$=1/(6D_R)$] of 34 ns at 20 °C for tRNA in 10 mM $MgCl_2$. The molecules have an axial ratio of 0.4 for the hydrodynamically equivalent ellipse of revolution, suggesting that our treatment on the basis of isotropic reorientation is too simplistic. While this is strictly true, the internal motion results will be only slightly altered by including

the anisotropy of overall motion.

Discussion

The key result of this work is the finding of conditions for significant incorporation of ^{13}C-labeled sugars into *E. coli* nucleic acids. Increased NMR signal levels permitted accurate relaxation data to be obtained on limited sample quantities over a wide frequency range, an important criterion for unraveling complex motion in macromolecules (Levy et al., 1981). For tRNA there is hope that purified isoaccepting species can be obtained in sufficient quantity to observe some single-carbon resonances, particularly with C1′ since the spread in chemical shifts is great. DNA as well as RNA is labeled in these experiments. Labeling of DNA at C1′ is particularly advantageous since the C1′ and C4′ signals overlap. Enrichment of either one permits their dynamical behavior to be sorted out.

On the basis of the present study of C1′ labeling, it appears quite feasible to enrich the other sugar carbons in nucleic acids as well. While there is some scrambling, each position should be largely carried through. Of course, this begs the nontrivial question of labeled ribose chemical synthesis, particularly for the interior carbons.

Relaxation times and NOE values for C1′ in *E. coli* tRNA are consistent with limited-amplitude internal motion of the C–H vectors having a correlation time of about 2 ns. This general result is in line with experimental studies of ^{13}C relaxation parameters for DNA double-helical fragments (Levy et al., 1981; Bolton & James, 1980a,b; Hogan & Jardetzky, 1979) and recent theoretical treatments of these data (Lipari & Szabo, 1981; Keepers & James, 1982). Work on ^{13}C relaxation in tRNA is more limited (Komoroski & Allerhand, 1972; Bolton & James, 1980a,b; Schmidt et al., 1980), and the data have not previously been analyzed in terms of restricted-amplitude internal motion for ribose carbons. Komoroski & Allerhand (1972) considered the ribose carbon T_1s to reflect the overall rotational motion and obtained a value of $\zeta_R = 30 \times 10^{-9}$ s for concentrated bulk yeast tRNA. Their natural abundance spectra were obtained at 15 MHz. Schmidt et al. (1980) incidentally measured ribose carbon T_1s at natural abundance in samples of *E. coli* tRNA where the C2 of adenine was enriched. NOEs were not obtained due to inadequate signal-to-noise levels. While the ribose T_1 values were consistent with isotropic rotation, they did indicate a faster correlation time (but still within experimental error) than that for the base carbons. Bolton & James (1980b) measured T_1 and NOE for yeast tRNA ribose carbons at 25.5 and 50.3 MHz. NOE values greater than 1.15 suggested that there must be internal motion of the sugar rings. They used a simple model of free internal diffusion to solve for ribose-carbon internal-motion correlation times over the range of (4–7) $\times$ 10^{-9} s.

Ribose carbons in these previous studies were not isotopically enriched, and the signal-to-noise ratios suffered accordingly. In contrast, the signal-to-noise level after enrichment enabled us to measure accurate T_1 and NOE values from 25 to 75 MHz, allowing for a more detailed interpretation, at a selected locus. Whichever restricted amplitude model one chooses, it is clear that the C1′–H bonds in tRNA have internal motion confined to a relatively small angle of excursion with correlation times on the order of 2 ns. It will be of great interest to do these experiments on tRNA labeled at the other ribose-carbon positions, particularly from the standpoint of amplitude of motion.

Given that the C1′ peak is not resolved into individual carbon resonances, there is some question about whether we are measuring a single relaxation time and NOE or an average. One might expect a range of flexibility for nucleotides, from those near the tightly knit hinge region to those on the 3′ end, for example. With bulk tRNA the whole C1′ resonance band relaxes with a single T_1 value, and the peak shapes are very close to the same with or without NOE, suggesting that there are not large numbers of C1′ carbons with widely differing internal dynamics. Interestingly, the Carr–Purcell experiment showed different transverse relaxation rates in parts of the peak with the upfield shoulder slower to relax than the bulk of carbons. T_2 is usually more sensitive to overall motional correlation times than T_1 or the NOE, possibly indicating a range of effective overall reorientation rates. This could arise if some molecules are aggregated [e.g., complementary anticodon binding (Eisinger, 1971)] or if some parts of a single tRNA have independent motion. Questions of this sort can be better addressed by examining purified single isoaccepting species of tRNAs, an approach that we are pursuing.

Acknowledgments

We are grateful to the Stable Isotope Resource at Los Alamos Scientific Laboratory for supplying the ^{13}C-labeled ribose. We thank Professor Warren Ford, Oklahoma State University, and Professor Dean A. Sherry, University of Texas, Dallas, for help in the multifrequency measurements. We acknowledge the important work of Julia G. Tompson in defining ^{13}C-enrichment conditions in general.

Registry No. Ribose, 50-69-1.

References

Agris, P. F., & Schmidt, P. G. (1980) *Nucleic Acids Res. 8*, 2085–2091.

Agris, P. F., Fujiwara, F. G., Schmidt, C. F., & Loeppky, R. N. (1975) *Nucleic Acids Res. 2*, 1503–1512.

Blakley, R. L., Cocco, L., London, R. E., Walker, T. E., & Matwiyoff, N. A. (1978) *Biochemistry 17*, 2284–2293.

Bolton, P. H., & James, T. L. (1979) *J. Phys. Chem. 83*, 3359–3363.

Bolton, P. H., & James, T. L. (1980a) *J. Am. Chem. Soc. 102*, 25–31.

Bolton, P. H., & James, T. L. (1980b) *Biochemistry 19*, 1388–1392.

Breitmaier, E., & Hollstein, U. (1976) *Org. Magn. Reson. 8*, 573–575.

Bull, T. E., Norne, J. E., Reimarsson, P., & Lindman, B. (1978) *J. Am. Chem. Soc. 100*, 4643–4647.

Davis, G. E., Gehrke, C. W., Kuo, K. C., & Agris, P. F. (1979) *J. Chromatogr. 173*, 281–298.

Dill, K., & Allerhand, A. (1979) *J. Am. Chem. Soc. 101*, 4376–4378.

Early, T. A., & Kearns, D. R. (1979) *Proc. Natl. Acad. Sci. U.S.A. 76*, 4165–4169.

Eisinger, J. (1971) *Biochem. Biophys. Res. Commun. 43*, 854–861.

Freeman, R., & Hill, H. (1975) in *Dynamic Nuclear Magnetic Resonance* (Jackman, L. M., & Cotton, F. A., Eds.) pp 131–162, Academic Press, New York.

Hogan, M. E., & Jardetzky, O. (1979) *Proc. Natl. Acad. Sci. U.S.A. 76*, 6341–6345.

Howarth, O. W. (1979) *J. Chem. Soc., Faraday Trans. 2 75*, 863–873.

Jelinski, L. W., & Torchia, D. A. (1980) *J. Biol. Chem. 138*, 255–272.

Keepers, J. W., & James, T. L. (1982) *J. Am. Chem. Soc. 104*, 929–939.

Komoroski, R. A., & Allerhand, A. (1972) *Proc. Natl. Acad. Sci. U.S.A. 69*, 1804–1808.
Kowalewski, J., & Levy, G. C. (1977) *J. Magn. Reson. 26*, 533–536.
Levitt, M., & Warshel, A. (1978) *J. Am. Chem. Soc. 100*, 2607–2613.
Levy, G. C., Hilliard, P. R., Jr., Levy, L. F., Rill, R. L., & Inners, R. (1981) *J. Biol. Chem. 256*, 9986–9989.
Lipari, G., & Szabo, A. (1980) *Biophys. J. 30*, 489–506.
Lipari, G., & Szabo, A. (1981) *Biochemistry 20*, 6250–6256.
London, R. E. (1980) in *Magnetic Resonance in Biology* (Cohen, J. S., Ed.) pp 1–69, Wiley, New York.
London, R. E., & Avitable, J. (1978) *J. Am. Chem. Soc. 100*, 7159–7165.
Moore, A. C., & Browne, D. T. (1980) *Biochemistry 19*, 5768–5773.
Otvos, J. D., & Browne, D. T. (1980) *Biochemistry 19*, 4011–4021.
Patkowski, A., & Chu, B. (1979) *Biopolymers 18*, 2051–2072.
Schmidt, P. G., Tompson, J. G., & Agris, P. F. (1980) *Nucleic Acids Res. 8*, 643–656.
Schweizer, M. P., Hamill, W. D., Jr., Walkiw, I. J., Horton, W. J., & Grant, D. M. (1980) *Nucleic Acids Res. 8*, 2075–2083.
Serianni, A. S., Nunez, H. A., & Barker, R. (1980) *J. Org. Chem. 45*, 3329–3341.
Tompson, J. G., & Agris, P. F. (1979) *Nucleic Acids Res. 7*, 765–779.
Tompson, J. G., Hayashi, F., Paukstellis, J. V., Loeppky, R. N., & Agris, P. F. (1979) *Biochemistry 18*, 2079–2085.
Wittebort, R. J., & Szabo, A. (1978) *J. Chem. Phys. 69*, 1722–1725.
Woessner, D. E. (1962) *J. Chem. Phys. 36*, 1–4.
Yokoyama, S., Usuki, K. M. J., Yamaizumi, Z., Nishimura, S., & Miyazawa, T. (1980) *FEBS Lett. 119*, 77–80.

Topological Arrangement of Four Functionally Distinct Domains in Hamster Plasma Fibronectin: A Study with Combination of S-Cyanylation and Limited Proteolysis†

Kiyotoshi Sekiguchi and Sen-itiroh Hakomori*

ABSTRACT: Hamster plasma fibronectin was shown previously to consist of four functionally distinct domains which were isolated as M_r 150 000–140 000, 40 000, 24 000, and 21 000 fragments (150K–140K, 40K, 24K, and 21K fragments) after mild thermolysin digestion [Sekiguchi, K., Fukuda, M., & Hakomori S. (1981) *J. Biol. Chem. 256*, 6452–6462]. The alignment of these domains and the location of cysteine residues have been studied by S-cyanylation of cysteine residues with 2-nitro-5-thiocyanobenzoic acid. Hamster plasma fibronectin contained 1.1 mol of cysteine residue/mol of subunit chain. This cysteine residue was localized in the 150K–140K domain. Cleavage of intact fibronectin at the cysteine residue by S-cyanylation produced three major fragments, i.e., sc155K, sc145K, and sc125K fragments (the prefix "sc" specifies the S-cyanylation-cleaved fragment). Only the sc145K fragment was heavily radiolabeled by factor XIIIa/[^{3}H]putrescine, as well as galactose oxidase/NaB^3H_4 for carbohydrates, indicating that it contained 24K and 40K domains which were located at the NH_2-terminal side of the cysteine residue. The sc145K fragment was separated from other fragments by gelatin–Sepharose chromatography, followed by gel filtration on Sephacryl S-200. Thermolysin digestion of the sc145K fragment produced 24K, 40K, and 55K fragments but did not produce the 21K fragment. The first two fragments represent NH_2-terminal 24K domain and a next adjacent carbohydrate-rich 40K domain, respectively. The 55K fragment was considered to represent COOH-terminal region of the sc145K fragment and overlap with NH_2-terminal portion of the 150K–140K domain, because this portion was obtained as an sc58K fragment by S-cyanylation of the 150K–140K domain. In contrast, thermolysin digestion of the S-cyanylation fragments, which were nonadsorbed on gelatin columns and were considered to be derived from the COOH-terminal portion of intact fibronectin, produced 64K, 62K, and 21K fragments, but not 24K or 40K. These results, taken together, indicate that the alignment of the four domains in the α subunit is NH_2–24K–40K–150K(–140K)–21K–COOH and that in the β subunit is NH_2–24K–40K–(150K–)140K–COOH.

Fibronectin is a multifunctional glycoprotein abundantly present in the pericellular matrix and in body fluids (Vaheri & Mosher, 1978; Yamada & Olden, 1978; Mosesson & Amrani, 1980; Pearlstein et al., 1980; Mosher, 1980; Ruoslahti et al., 1981a). A decrease or deletion of this protein associated on oncogenic transformation aroused a great deal of initial interest for the study of this protein (Gahmberg & Hakomori, 1973a; Hynes, 1973). It is an adhesive protein which mediates in vitro cell attachment and spreading onto uncoated or collagen-coated plastic surfaces (Klebe, 1974; Pearlstein, 1976; Grinnell, 1978). In plasma, it modulates the phagocytic activity of the reticuloendothelial system as a nonspecific opsonin (Saba et al., 1978). It shows an affinity toward various substances, including collagen (or gelatin), fibrin, glycosaminoglycans, bacterial surface components, actin, and de-

† From the Program of Biochemical Oncology, Fred Hutchinson Cancer Research Center, and Departments of Pathobiology, Microbiology, and Immunology, School of Public Health and School of Medicine, University of Washington, Seattle, Washington 98104. *Received May 18, 1982; revised manuscript received November 5, 1982.* This investigation was supported by Research Grant CA23907 from the National Institutes of Health. A part of the present investigation was presented at the 21st Annual Meeting of the American Society for Cell Biology at Anaheim, CA (Sekiguchi & Hakomori, 1981).

* Address correspondence to this author at the Program of Biochemical Oncology, Fred Hutchinson Cancer Research Center.

0006-2960/83/0422-1415$01.50/0